Accelerated optimization of transparent, amorphous zinc-tin-oxide thin films for optoelectronic applications

Matthew J. Wahila, Zachary W. Lebens-Higgins, Keith T. Butler, Daniel Fritsch, Robert E. Treharne, Robert G. Palgrave, Joseph C. Woicik, Benjamin J. Morgan, Aron Walsh, and Louis F. J. Piper

---

Accelerated optimization of transparent, amorphous zinc-tin-oxide thin films for optoelectronic applications

View Online   Export Citation   CrossMark

Matthew J. Wahila,[1] (iD) Zachary W. Lebens-Higgins,[1] Keith T. Butler,[2,a] (iD) Daniel Fritsch,[3] (iD) Robert E. Treharne,[4] Robert G. Palgrave,[5] Joseph C. Woicik,[6] Benjamin J. Morgan,[2] (iD) Aron Walsh,[7] (iD) and Louis F. J. Piper[8,b] (iD)

AFFILIATIONS

[1] Department of Physics, Applied Physics and Astronomy, Binghamton University, Binghamton, New York 13902, USA
[2] Department of Chemistry, University of Bath, Claverton Down, Bath BA2 7AY, United Kingdom
[3] Department Structure and Dynamics of Energy Materials, Helmholtz-Zentrum Berlin für Materialien und Energie, Hahn-Meitner-Platz 1, 14109 Berlin, Germany
[4] Stephenson Institute for Renewable Energy, University of Liverpool, Liverpool L69 7ZF, United Kingdom
[5] University College London, Department of Chemistry, 20 Gordon Street, London WC1H 0AJ, United Kingdom
[6] Materials Science and Engineering Laboratory, National Institute of Standards and Technology, Gaithersburg, Maryland 20899, USA
[7] Department of Materials, Imperial College London, Exhibition Road, London SW7 2AZ, United Kingdom
[8] Materials Science and Engineering, Binghamton University, Binghamton, New York 13902, USA

[a] Current address: ISIS Neutron and Muon Source, Rutherford Appleton Laboratories, Didcot OX11 0QX, United Kingdom.
[b] Electronic mail: lpiper@binghamton.edu

ABSTRACT

In the last decade, transparent amorphous oxide semiconductors (TAOS) have become an essential component of many electronics, from ultra high resolution displays to solar cells. However, these disordered oxides typically rely on expensive component metals like indium to provide sufficient charge carrier conduction, and their optoelectronic properties are not as predictable and well-described as those of traditional, crystalline semiconductors. Herein we report on our comprehensive study of the amorphous zinc-tin-oxide (a-ZTO) system for use as an indium-free, n-type TAOS. Using a combination of high-throughput co-deposition growth, high resolution spectral mapping, and atomistic calculations, we explain the development of disorder-related subgap states in SnO_2-like a-ZTO and optical bandgap reduction in ZnO-like a-ZTO. In addition, we report on a composition-induced electronic and structural transition in ZnO-like a-ZTO resulting in an exceptionally high figure of merit, comparable to that of amorphous indium-gallium-zinc-oxide. Our results accelerate the development of a-ZTO and similar systems as indium-free TAOS materials.

Transparent amorphous oxide semiconductors (TAOS) are currently of great interest due to the wide range of optoelectronic applications enabled by their high transparencies and charge carrier mobilities combined with their potential for low temperature fabrication on inexpensive substrates.[1] TAOS systems that incorporate multiple cation species are particularly promising as they offer the ability to fine tune optoelectronic properties for specific applications by varying the atomic composition and coordination.[2–7] Unfortunately, most TAOS systems investigated thus far incorporate rare, expensive, and/or toxic cations such as indium, hindering their development and reducing their practicality.[8] Finding

a material system with similar performance to the prototypical TAOS, amorphous indium–gallium–zinc-oxide (a-IGZO),[2] but composed of only inexpensive, abundant, and non-toxic elements would represent a substantial advancement in the development of TAOS materials.

Amorphous zinc-tin-oxide (a-ZTO), which possesses many desirable properties for thin film transistor applications, has recently arisen as a potential a-IGZO alternative.[9,10] ZTO films contain only inexpensive and innocuous elements and can be fabricated using a wide variety of industrially relevant methods, including sol-gel,[11] magnetron sputtering,[7,12–15] chemical vapor,[16] pulsed laser,[17] and atomic layer depositions.[9,18,19] Some researchers have even employed co-deposition techniques to quickly fabricate large sample sets and accelerate investigation of the large compositional phase space.[7,12,20,21] However, most of these studies have focused on the optimization of films for specific device applications rather than attempting to explain the physical origins of the evolving material properties.

Recent research has focused predominantly on the effects of post-growth anneal treatments, compositional variations, and material interactions on the properties of complete electronic devices, rather than investigating the underlying physics of the amorphous ZTO system.[6,7,22–27] Several recent studies have begun to investigate the effects of composition and disorder on the electronic structure of ZTO;[17,19,28] however, the full range of possible cation ratios has remained unexplored and the atomistic origin of many optical and electronic properties of these ZTO films remains uncertain.

Herein, we present our study of the a-ZTO system using co-deposition of thin films in tandem with multiple optical and x-ray techniques, including ellipsometry and synchrotron-based hard x-ray photoelectron spectroscopy (HAXPES). Our high-resolution electronic and optical property mapping elucidates the evolution of electronic structure across a wide range of compositions, helping to identify and correlate key phenomena occurring across the a-ZTO compositional phase space. Combining our experimental results with density functional theory (DFT) calculations, we then explain these phenomena in terms of the local structure and atomic coordination within these structurally disordered films.

In order to thoroughly investigate the a-ZTO system, thin films were deposited on 10×10 cm OptiWhite soda-lime glass by room temperature, magnetron sputtering co-deposition at the University of Liverpool, as depicted in Fig. 1. Powers of 250 and 80 W were applied to the ZnO and SnO_2 sputter guns, respectively, under a 5 mTorr Ar atmosphere. These large samples were then cut into smaller pieces for easier experimental characterization (see Fig. 1 of the supplementary material). This fabrication method produces a continuous compositional gradient across the deposition area, allowing for the simultaneous investigation of a large swath of the compositional phase space.[7,12,20,21] Amorphous SnO_2 and polycrystalline ZnO films were fabricated for reference using single target depositions with the same parameters.
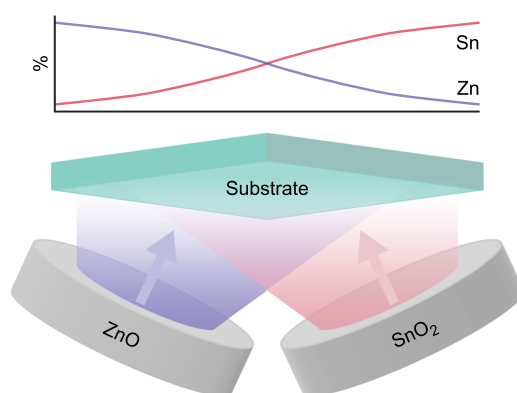

FIG. 1. **Co-deposition method.** Schematic showing how the co-deposition process creates a continuous compositional gradient across the film deposition area.

Figures 2(a) and 2(b) show the variation in cation ratio and film thickness across the 10×10 cm film resulting from the co-deposition. The compositional map, shown in Fig. 2(a), was created from scanning x-ray photoelectron spectroscopy (XPS) core-level spectra performed on 256 points across the sample area using a laboratory-based monochromated Al Kα source with a hemispherical analyzer located at University College London. Measurements were performed in constant analyzer energy mode with a pass energy of 50 eV. The Sn:Zn ratio was found to vary smoothly from a minimum of 9.23% tin on the bottom-left to a maximum of 75.30% tin on the top-right.

The film thickness map, shown in Fig. 2(b), was created using ellipsometry measurements taken on an 81 point measurement grid across the central 8×8 cm^2 portion of the sample area using a Woollam Co. spectroscopic ellipsometer at the University of Liverpool. The observed compositional gradient and thickness variations from this co-deposition compare well with trends predicted using ellipsometry on single target deposition films (see Figs. 2 and 3 of the supplementary material).

The optical bandgap evolution, shown in Fig. 2(c), was determined using the Tauc analysis of ultraviolet-visible spectroscopy (UV-Vis) measurements taken at 83 points across the sample area using either a Filmetrics F20 series reflectometer with T-1-UV transmittance upgrade or a Shimadzu UV-1800 UV-Vis spectrophotometer, both located at Binghamton University.[29] Additional analysis was performed on the UV-Vis spectra to estimate film thicknesses and indices of refraction for comparison with the ellipsometry results (see Fig. 4 of the supplementary material).[30,31] Interestingly, the optical bandgap evolution does not directly correspond to film composition, with the high tin percentage corner of the sample displaying an almost constant optical bandgap independent of composition, while the low tin percentage corner displays a steep drop in bandgap size with decreasing tin content (see Fig. 5 of the supplementary material).
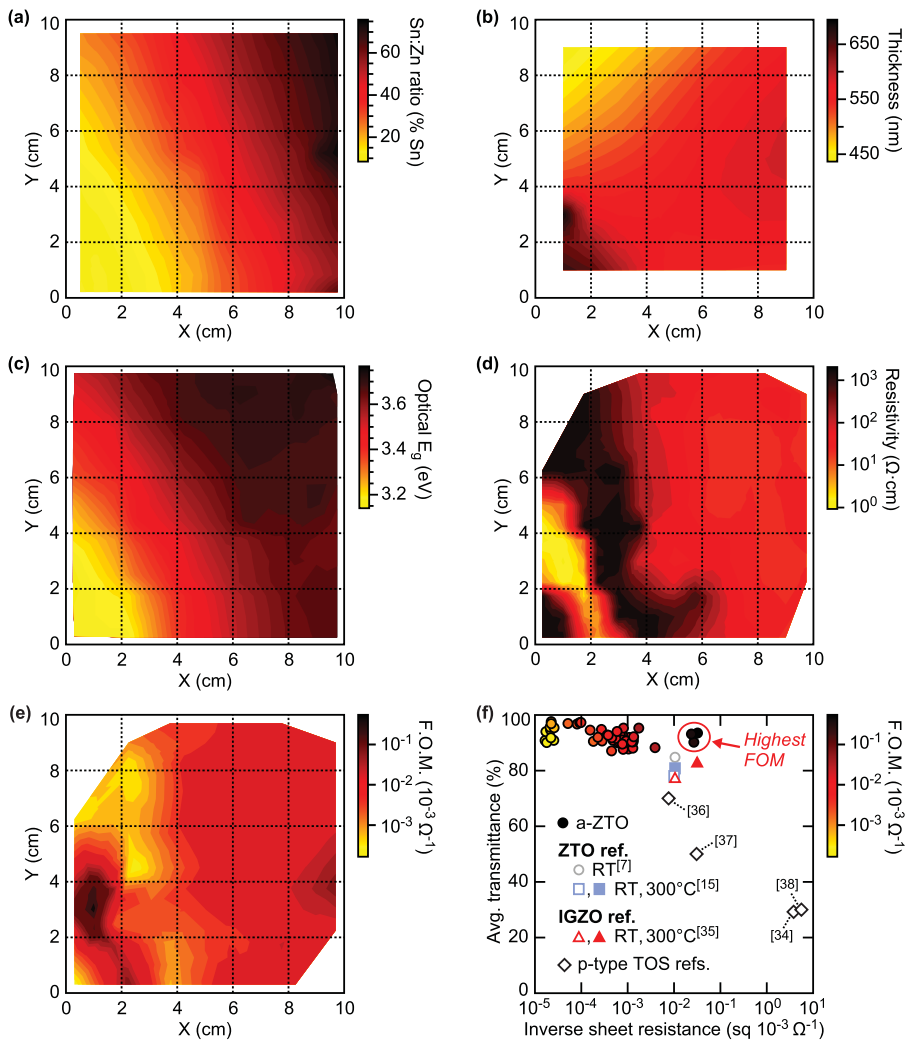
FIG. 2. **Film characterization across the co-deposition area.** Contour maps of (a) Sn:Zn ratio, (b) film thickness, (c) direct optical bandgap, (d) resistivity, and (e) figure of merit across the 10 × 10 cm a-ZTO thin film deposition area. (f) Graphical representation of electrical resistance, optical transmission, and FOM for points across the a-ZTO film, including reference points from the literature for comparable ZTO (gray circle and blue squares) and IGZO (red triangles) sputtered thin films, as well as high-quality, crystalline p-type TAOS films (black diamonds).

Film resistivity, shown in Fig. 2(d), was calculated for 131 points across the sample area using sheet resistances measured with a 4-point probe system located in the Nanofabrication Facility at Binghamton University and film thicknesses were calculated from ellipsometry (see Fig. 6 of the supplementary material). There are significant variations in resistivity across the sample which can be correlated to both the film thickness and Sn:Zn ratio. While the film thickness does have an effect on the resistivity, it follows the expected trend of thinner regions displaying higher resistivity than thicker regions when the Sn:Zn ratio is constant. The more interesting trends are attributable to the films' Sn:Zn ratio. While the high tin percentage corner of the sample has a fairly uniform resistivity between 10 and 100 Ω cm, both the highest (>2000 Ω cm) and lowest (<1 Ω cm) resistivities are found near the low tin percentage corner. Of particular interest is the region of ~10%–12% tin, where film resistivity is drastically lower than

that of neighboring regions with slightly more or less tin content.

Figure of Merit (FOM) values were calculated for points across the a-ZTO film, as shown in Fig. 2(e). The FOM of a thin film can be calculated using the formula FOM = σ/α, where σ is the film conductivity and α is the optical absorption coefficient. If optical reflectance is negligible, this can be approximated by FOM $\approx -1/R_S \ln(T)$, where R_S is the sheet resistance and T is the wavelength-averaged optical transmittance.[32–34] Although optical transparency across the entire a-ZTO film is extremely high, much of the film is too resistive to result in a reasonable FOM. However, the previously mentioned region of ~10%–12% tin possesses a low enough resistance to give FOM values comparable to or better than previously reported values for a-ZTO and other high FOM TAOS materials.[7,15,35]

Shown in Fig. 2(f), the best resistivity values reported in the literature for a-ZTO have remained fairly constant

for many years.[7,15] Surprisingly, our low tin percentage a-ZTO possesses both better transparency and better resistivity than previously reported for high tin percentage a-ZTO films. Additionally, although Hall measurements are not well suited to investigate non-uniform and amorphous films, some Hall measurements were performed on select 1 × 1 cm film pieces. The results indicate that our low resistivity, low tin percentage region possesses a Hall mobility and bulk concentration comparable to those of our high tin percentage region despite having a several orders of magnitude higher conductivity (see Fig. 7 of the supplementary material).

While higher temperature fabrication up to 300 °C has been found to produce slightly increased transparency in high tin percentage a-ZTO films, it has not led to significantly improved resistivity.[15] This puts high tin percentage a-ZTO at a distinct disadvantage to a-IGZO, which has been shown to have both improved electronic and optical properties following low-temperature processing.[5] By contrast, our low tin percentage a-ZTO is found to already possess a better FOM than some a-IGZO reported in the literature which was annealed up to 300 °C.[35]

Additionally, our a-ZTO also compares favorably to transparent, crystalline p-type oxides such as CuAlO$_2$,[36] ZnRh$_2$O$_4$,[37] CuCrO,[38] and SrCrO.[34] These crystalline p-type materials are able to match or even surpass amorphous n-types in terms of resistivity but at the cost of significantly reduced optical transparency due to subgap states or disruption of the mechanisms responsible for their large optical bandgaps. By contrast, while our low tin-percentage a-ZTO does possess a slightly smaller optical bandgap than our high tin percentage film, the gap remains larger than 3 eV across the entire deposition area, resulting in excellent optical transparency at all compositions.

From these results, we note two compositional regions warranting further investigation: the top-right corner possessing 60% tin or more (tin-rich) and the bottom-left corner possessing 30% tin or less (tin-poor). The tin-rich film possesses a large optical bandgap and reasonable resistivity which both remain fairly constant over a large compositional range, indicating that tin-rich a-ZTO could make a good TAOS material as suggested by other studies.[7,21] By contrast, the tin-poor film possesses a rapidly changing optical bandgap and both the highest and lowest observed resistivity. Understanding the origin of the anomalously low resistivity in this region could lead to the development of inexpensive ZTO-based materials for transparent conducting oxide (TCO) applications.[39,40]

Tauc plots for points along a diagonal between the tin-rich and tin-poor corners of the deposition area are shown in Fig. 3(a), including plots for reference amorphous SnO$_2$ (a-SnO$_2$) and polycrystalline ZnO (c-ZnO). For comparison, Tauc plots were also created using optical constants calculated with hybrid DFT (see Fig. 8 of the supplementary material).[41] The bandgap of the a-ZTO film is found to increase as tin concentration increases, with the a-SnO$_2$ reference clearly possessing the largest optical bandgap. Additionally, a broadening of the absorption edge is observed in all of the a-ZTO and a-SnO$_2$ spectra, which is mostly consistent with exponential Urbach tail absorption due to structural disorder.[42,43] However, the more tin-rich a-ZTO and a-SnO$_2$ display additional absorption below the main absorption edge (indicated by a red arrow), which is likely due to more than just Urbach tailing.

To investigate the tendency of tin-rich a-ZTO to form defect associated subgap states, hard x-ray photoelectron spectroscopy (HAXPES) measurements were performed at the
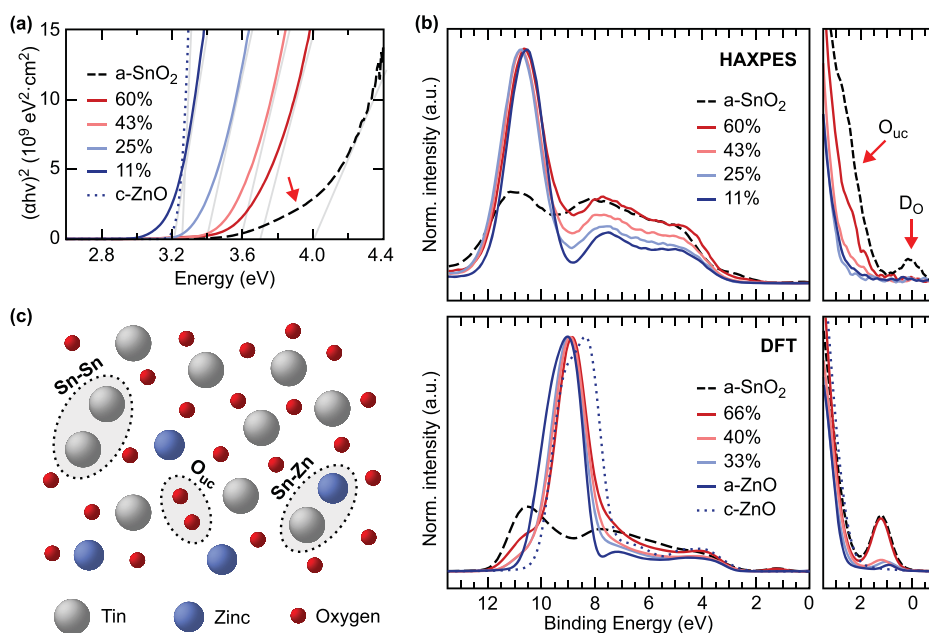
FIG. 3. **Subgap state formation in tin-rich a-ZTO.** (a) Tauc plots for select points from high to low tin composition, including c-ZnO and a-SnO$_2$ for reference. (b) HAXPES valence band spectra and DFT total density of states after weighting and convolution for several compositions of a-ZTO, including a-SnO$_2$ and c/a-ZnO for reference. Under-coordinated oxygen (O$_{uc}$) and oxygen deficiency (D$_O$) related subgap states are identified. (c) Simplistic diagram of potential under-coordinated oxygen and oxygen deficiency defects within the a-ZTO.

National Institute of Standards and Technology (NIST) bending magnet beamline X24 at the National Synchrotron Light Source (NSLS) at Brookhaven National Laboratory. Measurements were performed at an ~4 keV photon energy, with a pass energy of 500 eV and a Gaussian instrumental broadening of 0.45 eV. Energy calibration of the HAXPES spectra was performed using external Au references in electrical contact with the samples.

For comparison, density functional theory calculations were performed for several stoichiometric a-ZTO compositions. Structures were first generated using a melt and quench approach, previously demonstrated to provide good agreement with experimental results.[44,45] Starting from an initial crystal structure of each composition, the system was heated to 3000 K using molecular dynamics (MD) and allowed to evolve for 10 ps, using a time step of 0.5 fs. Following the melting, the resultant systems were cooled to 0 K at a rate of 5×10^{13} K s^{-1}. The structures were then allowed to relax until the forces on all atoms were below a threshold value of 0.005 eV Å^{-1}.

The DFT calculations were performed in the Vienna *Ab Initio* Simulation Package (VASP)[46] within the projector augmented wave formalism,[47] using gamma point sampling, the PBEsol functional,[48] and a cutoff energy of 400 eV. The final valence band density of states (DOS) were then produced by weighting each partial DOS with the appropriate photoionization cross section, summing the partial DOS together, and then applying a pseudo-Voigt profile convolution to match experimental broadening. The calculated spectra were then energetically aligned to the experimental spectra for comparison. It must be noted that while the Zn 3d semi-core level peak position is clearly underestimated by the DFT, this is to be expected due to the lack of explicit on-site corrections in the calculations.[49] This misplacement of the Zn 3d should not significantly affect the calculated density of states near the valence and conduction band edges.

Both the HAXPES and DFT total DOS of the valence band, shown in Fig. 3(b), confirm the tendency of tin-rich a-ZTO to form defect associated subgap states. Both midgap states and near-edge states immediately above the valence band edge are observed for only the more tin-rich a-ZTO compositions, with HAXPES spectra for the tin-poor compositions showing no evidence of subgap states. These coordination-related subgap states are likely the cause of the additional optical absorption observed below the main absorption edge of the tin-rich compositions.

Previous theoretical and experimental work has confirmed that these subgap states originate from the local coordination of cation (tin/zinc) and anion (oxygen) atoms within the disordered structure, as depicted in Fig. 3(c).[44,50-53] These defect states can exist in perfectly stoichiometric films provided there is enough variation in atomic coordination environments. Moreover, work on a-IGZO has shown that it is possible to modify or even remove these defect states by adjusting local atomic coordinations with only low temperature processing.[5] The possibility of achieving a similar control of subgap states within tin-rich a-ZTO makes it an excellent candidate for further material optimization.

On the other end of the compositional phase space, tin-poor a-ZTO displays intriguing behavior which has yet to be explored. In general, the tin-rich film possesses reasonable resistivity, while the tin-poor film possesses very high resistivity, as shown in Fig. 2(d). However, the sudden drop in resistivity near 10%–12% tin is an anomaly. This low resistivity gives the tin-poor a-ZTO film an unusually high FOM for an amorphous oxide semiconductor.[32-34] One indication of why this compositional region displays unexpectedly low resistivity is given in Fig. 4.

Figure 4(a) shows x-ray diffraction (XRD) spectra taken on points across the tin-poor corner of the deposition area using a PANalytical X'Pert PRO XRD system located in the Analytical and Diagnostics Laboratory (ADL) at Binghamton University. A weak XRD feature near 33.5° is found to appear between ~25% and 11% tin and grows more intense as tin percentage is further reduced. The c-ZnO reference film grown using the same deposition parameters exhibits a large ZnO (002) peak at a slightly higher diffraction angle, suggesting that the feature observed in the tin-poor a-ZTO could be due to the formation of some strained ZnO crystallites.[12,20] However, as shown
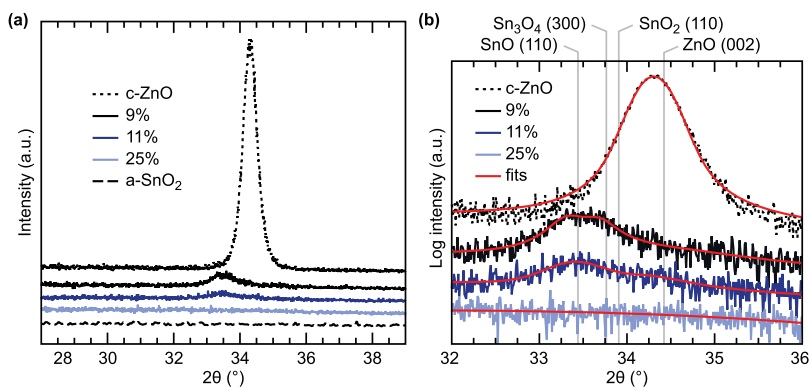

FIG. 4. **Crystallite formation in tin-poor a-ZTO.** (a) XRD spectra for select points across the tin-poor corner, including a c-ZnO and a-SnO$_2$ references. Spectra have been truncated to only show the region containing observed features. (b) Truncated XRD including curve fits.
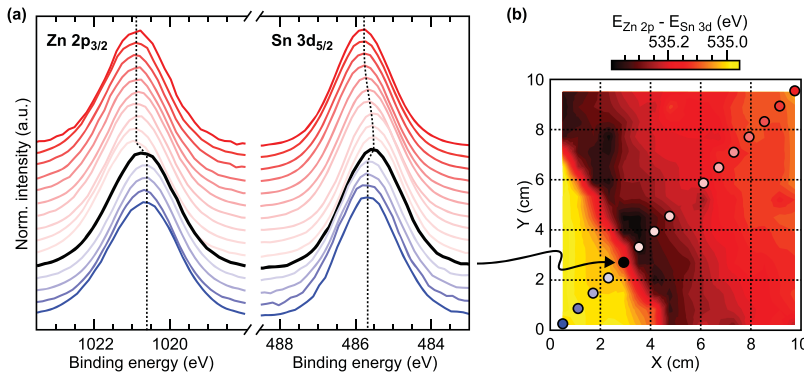
FIG. 5. **Peak shifts in tin-poor a-ZTO.** (a) Example Zn $2p_{3/2}$ and Sn $3d_{5/2}$ XPS spectra for select points from high to low tin percentages. (b) Contour map of the Zn 2p–Sn 3d core-level energetic separation across the entire deposition area.

in Fig. 4(b), this weak feature appears to be made up of more than one peak for at least some compositions and could also be due to segregated Sn_xO_y crystallites of different compositions within the tin-poor a-ZTO matrix.[44]

Shown in Fig. 5(a), Zn 2p and Sn 3d XPS core levels taken from select spots across the deposition area display compositionally dependent shifts that correlate with the observed crystallite formation. Commensurate shifts are also observed in the near-valence Zn 3d and Sn 4d levels as well as auger peaks measured using both high-resolution XPS and HAX-PES (see Figs. 9–11 of the supplementary material). The Zn 2p peak displays an abrupt energetic shift toward the Fermi level within the composition range where weak XRD peaks begin to appear. This shift indicates a sudden and sustained change in the local zinc bonding environment with the onset of crystallization and agrees with the expected behavior of the Zn 3d upon crystallization as predicted by DFT, as shown in Fig. 3(b). Concurrently, the Sn 3d peak displays a gradual energetic shift toward the Fermi level as the film composition approaches the onset of crystallization, abruptly returning to its original energetic position once some weak crystallization is observed.

Figure 5(b) maps the evolution of the Zn 2p and Sn 3d core level separation across the entire deposition area. Plotting core level separation rather than individual peak positions removes any contribution from Fermi level shifts or other confounding effects, providing clearer insight into changes in the local environment around cation species. The core level separation is found to gradually increase by ~0.3 eV between 40% and 20% tin and then abruptly decrease in the ~25%–11% tin range where initial crystallization is observed. This smaller separation is then maintained for the entire tin-poor corner of the film.

Figure 6 shows three important optoelectronic properties as a function of film Sn:Zn ratio, i.e., optical bandgap, film resistivity, and energetic separation of key cation core levels. The evolution of these properties highlights important local disorder-related phenomena that must be taken into account when developing a-ZTO thin films for different applications.

The optical bandgap evolution of disordered ZTO, shown in Fig. 6(a), displays bandgap reduction at both compositional ends (indicated by the red arrows). The observed bandgap
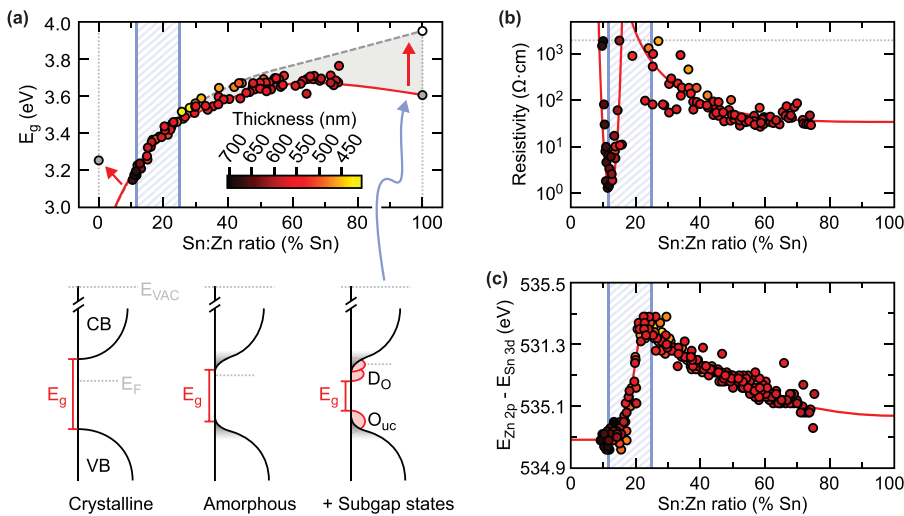

FIG. 6. Summary of the observed optoelectronic phenomena. (a) Evolution of the direct optical bandgap with the Sn:Zn ratio, including a-SnO$_2$ and c-ZnO endpoints. Bandgap trends including (red line) and excluding (gray dashed line) subgap absorption are extrapolated to the a-SnO$_2$ endpoint determined by both including (gray circle) and excluding (white circle) weak absorption tailing. (b) Evolution of film resistivity with the Sn:Zn ratio, only including points with resistivity below the maximum value measurable by our equipment (dotted gray line). (c) Evolution of the Zn 2p–Sn 3d energetic separation with the Sn:Zn ratio. For all plots, trends are extrapolated across the full Sn:Zn ratio range (red line) and the compositional region wherein weak crystallization begins is indicated (blue hatching).

changes are confirmed using both optical transmittance and ellipsometry measurements (see Fig. 12 of the supplementary material). Local coordination defects, which can play a large role in reducing optical transparency through sub-gap state absorption, are far more likely at SnO_2-like (tin-rich) compositions due to the higher oxygen to cation ratio. These defect states and their corresponding optical absorption are clearly observed with increasing magnitude as the tin content increases, up to and including the pure a-SnO_2 endpoint. The ability to control these defects is integral to the further development of tin-rich a-ZTO for applications where high optical transparency is desired.

While disordered ZnO-like (tin-poor) compositions can also suffer from bandgap reduction compared to the c-ZnO endpoint, this is not attributed to under-coordinated oxygen- or cation-related defect states as it is for SnO_2-like compositions. Instead, first-principles simulations suggest the cause to be band edge changes resulting from altered Zn 4s–O 2p hybridization in the disordered phase (see Fig. 13 of the supplementary material). Disorder in pure ZnO has been suggested to decrease Zn 4s–O 2p hybridization, resulting in a lower intersite hopping probability and more localized Zn 4s conduction states.[54,55] This localization would curtail percolation/hopping conduction through the film, greatly increasing resistivity.[2,4] This is in contrast to a-SnO_2, where high mobilities comparable to that of the crystalline phase are known to be achievable.[56] Thus, more ZnO-like compositions might be expected to possess lower electron mobilities than more SnO_2-like compositions.

Figure 6(b) shows the resistivity changes with composition, mostly confirming the expected trend of disordered SnO_2-like (tin-rich) compositions being far less resistive than the disordered ZnO-like (tin-poor) compositions. However, it also reveals the anomalous drop in resistivity at certain low tin concentrations, which correlates with the observed onset of weak crystallization. Furthermore, this onset of weak crystallization strongly correlates with the sudden shifts in relative core-level peak positions measured using XPS/HAXPES, as shown in Fig. 6(c). Taken together, all of these data point toward a transition between two discrete material regimes with markedly different local atomic interactions occurring around a 20% tin to zinc ratio.

In summary, using thin film co-deposition in conjunction with high-resolution spatial mapping of film properties, we have correlated the observed evolution of optoelectronic properties with changes in the local electronic and atomic structures. In addition to clarifying the cause and effects of subgap state formation on film properties across a wide compositional range, we have also revealed a thus far unreported composition-induced electronic transition in tin-poor amorphous zinc-tin-oxide, which results in high figure of merit values comparable to room temperature grown a-IGZO.

While disorder in these multi-cation oxides typically results in poor charge carrier conduction, the observed electronic transition represents an unexpected exception.

Contrary to conventional wisdom, whereby one might expect the greatest conduction to occur at tin-rich compositions due to the spherical tin 5s orbital contributions in the conduction band, the observed electronic and structural changes instead result in a narrow range of tin-poor compositions possessing a drastically increased conduction. Understanding these material behaviors, both expected and unexpected, is critically important for the further development of amorphous zinc-oxide based semiconductors for electronics applications.

See supplementary material for additional details on the film growth method, details on the optical analysis, comparison between UV-Vis and ellipsometry results, comparison between theoretical and experimental Tauc plots, additional XPS/HAXPES spectra, and valence band partial density of states from DFT calculations.

REFERENCES

[1] X. Yu, T. J. Marks, and A. Facchetti, "Metal oxides for optoelectronic applications," Nat. Mater. **15**, 383–396 (2016).

[2] K. Nomura, H. Ohta, A. Takagi, T. Kamiya, M. Hirano, and H. Hosono, "Room-temperature fabrication of transparent flexible thin-film transistors using amorphous oxide semiconductors," Nature **432**, 488 (2004).

[3] T. Kamiya, K. Nomura, and H. Hosono, "Origins of high mobility and low operation voltage of amorphous oxide TFTs: Electronic structure, electron transport, defects and doping," J. Disp. Technol. **5**, 273–288 (2009).

[4] T. Kamiya and H. Hosono, "Material characteristics and applications of transparent amorphous oxide semiconductors," NPG Asia Mater. **2**, 15 (2010).

[5] S. Sallis, K. T. Butler, N. F. Quackenbush, D. S. Williams, M. Junda, D. A. Fischer, J. C. Woicik, N. J. Podraza, B. E. White, A. Walsh, and L. F. J. Piper, "Origin of deep subgap states in amorphous indium gallium zinc oxide: Chemically disordered coordination of oxygen," Appl. Phys. Lett. **104**, 232108 (2014).

[6] K. M. Niang, J. Cho, S. Heffernan, W. I. Milne, and A. J. Flewitt, "Optimisation of amorphous zinc tin oxide thin film transistors by remote-plasma reactive sputtering," J. Appl. Phys. **120**, 085312 (2016).

[7] M. Morales-Masis, F. Dauzou, Q. Jeangros, A. Dabirian, H. Lifka, R. Gierth, M. Ruske, D. Moet, A. Hessler-Wyser, and C. Ballif, "An indium-free anode

for large-area flexible OLEDs: Defect-free transparent conductive zinc tin oxide," Adv. Funct. Mater. **26**, 384–392 (2016).

[8]E. Nakamura and K. Sato, "Managing the scarcity of chemical elements," Nat. Mater. **10**, 158–161 (2011).

[9]J. Heo, S. Bok Kim, and R. G. Gordon, "Atomic layer deposited zinc tin oxide channel for amorphous oxide thin film transistors," Appl. Phys. Lett. **101**, 113507 (2012).

[10]W. B. Jackson, R. L. Hoffman, and G. S. Herman, "High-performance flexible zinc tin oxide field-effect transistors," Appl. Phys. Lett. **87**, 193503 (2005).

[11]S.-M. Lee, Y.-H. Joo, and C.-I. Kim, "Influences of film thickness and annealing temperature on properties of sol-gel derived ZnO-SnO$_2$ nanocomposite thin film," Appl. Surf. Sci. **320**, 494–501 (2014).

[12]J. H. Ko, I. H. Kim, D. Kim, K. S. Lee, T. S. Lee, B. Cheong, and W. M. Kim, "Transparent and conducting Zn-Sn-O thin films prepared by combinatorial approach," Appl. Surf. Sci. **253**, 7398–7403 (2007).

[13]I.-J. Lee, N.-E. Sung, K. H. Chae, and R. Conley, "Characterization of zinc-tin-oxide films deposited by radio frequency magnetron sputtering at various substrate temperatures," Thin Solid Films **548**, 385–388 (2013).

[14]T. Moriga, Y. Hayashi, K. Kondo, Y. Nishimura, K.-i. Murai, I. Nakabayashi, H. Fukumoto, and K. Tominaga, "Transparent conducting amorphous Zn-Sn-O films deposited by simultaneous dc sputtering," J. Vac. Sci. Technol., A **22**, 1705–1710 (2004).

[15]T. Minami, H. Sonohara, S. Takata, and H. Sato, "Highly transparent and conductive zinc-stannate thin films prepared by RF magnetron sputtering," Jpn. J. Appl. Phys., Part 2 **33**, L1693–L1696 (1994).

[16]J. Park, K. T. Oh, D. H. Kim, H. J. Jeong, Y. C. Park, H. S. Kim, and J. S. Park, "High-performance zinc tin oxide semiconductor grown by atmospheric-pressure mist-CVD and the associated thin-film transistor properties," ACS Appl. Mater. Interfaces **9**, 20656–20663 (2017).

[17]M. K. Jayaraj, K. J. Saji, K. Nomura, T. Kamiya, and H. Hosono, "Optical and electrical properties of amorphous zinc tin oxide thin films examined for thin film transistor application," J. Vac. Sci. Technol., B: Microelectron. Nanometer Struct. **26**, 495 (2008).

[18]M. Kapilashrami, C. X. Kronawitter, T. Torndahl, J. Lindahl, A. Hultqvist, W.-C. Wang, C.-L. Chang, S. S. Mao, and J. Guo, "Soft x-ray characterization of Zn$_{1-x}$Sn$_x$O$_y$ electronic structure for thin film photovoltaics," Phys. Chem. Chem. Phys. **14**, 10154–10159 (2012).

[19]S. C. Siah, S. W. Lee, Y. S. Lee, J. Heo, T. Shibata, C. U. Segre, R. G. Gordon, and T. Buonassisi, "X-ray absorption spectroscopy elucidates the impact of structural disorder on electron mobility in amorphous zinc-tin-oxide thin films," Appl. Phys. Lett. **104**, 242113 (2014).

[20]J. D. Perkins, J. A. del Cueto, J. L. Alleman, C. Warmsingh, B. M. Keyes, L. M. Gedvilas, P. A. Parilla, B. To, D. W. Readey, and D. S. Ginley, "Combinatorial studies of Zn-Al-O and Zn-Sn-O transparent conducting oxide thin films," Thin Solid Films **411**, 152–160 (2002).

[21]J. S. Kim, J. K. Park, Y. J. Baik, W. M. Kim, J. Jeong, and T. Y. Seong, "Electrical, optical and etching properties of Zn-Sn-O thin films deposited by combinatorial sputtering," J. Korean Phys. Soc. **61**, 1651–1655 (2012).

[22]P. Görrn, P. Hölzer, T. Riedl, W. Kowalsky, J. Wang, T. Weimann, P. Hinze, and S. Kipp, "Stability of transparent zinc tin oxide transistors under bias stress," Appl. Phys. Lett. **90**, 063502 (2007).

[23]P. Görrn, M. Lehnhardt, T. Riedl, and W. Kowalsky, "The influence of visible light on transparent zinc tin oxide thin film transistors," Appl. Phys. Lett. **91**, 193504 (2007).

[24]W. Hu and R. L. Peterson, "Molybdenum as a contact material in zinc tin oxide thin film transistors," Appl. Phys. Lett. **104**, 192105 (2014).

[25]J. Jang, D. G. Kim, D. M. Kim, S.-J. Choi, J.-H. Lim, J.-H. Lee, Y.-S. Kim, B. D. Ahn, and D. H. Kim, "Investigation on the negative bias illumination stress-induced instability of amorphous indium-tin-zinc-oxide thin film transistors," Appl. Phys. Lett. **105**, 152108 (2014).

[26]M. G. McDowell, R. J. Sanderson, and I. G. Hill, "Combinatorial study of zinc tin oxide thin-film transistors," Appl. Phys. Lett. **92**, 013502 (2008).

[27]A. Marette, A. Poulin, N. Besse, S. Rosset, D. Briand, and H. Shea, "Flexible zinc-tin oxide thin film transistors operating at 1 kV for integrated switching of dielectric elastomer actuators arrays," Adv. Mater. **29**, 1–6 (2017).

[28]J. Lee, D.-Y. Cho, J. Jung, U. Ki Kim, S. Ho Rha, C. Seong Hwang, and J.-H. Choi, "Theoretical and experimental studies on the electronic structure of crystalline and amorphous ZnSnO$_3$ thin films," Appl. Phys. Lett. **102**, 242111 (2013).

[29]J. I. Pankove, *Optical Processes in Semiconductors* (Dover Publications, Inc., 1971).

[30]R. Swanepoel, "Determination of the thickness and optical constants of amorphous silicon," J. Phys. E: Sci. Instrum. **16**, 1214–1222 (1983).

[31]W. L. Bond, "Measurement of the refractive indices of several crystals," J. Appl. Phys. **36**, 1674–1677 (1965).

[32]R. G. Gordon, "Criteria for choosing transparent conductors," MRS Bull. **25**, 52–57 (2000).

[33]E. Arca, K. Fleischer, and I. V. Shvets, "Magnesium, nitrogen codoped Cr$_2$O$_3$: A p-type transparent conducting oxide," Appl. Phys. Lett. **99**, 111910 (2011).

[34]K. H. L. Zhang, Y. Du, A. Papadogianni, O. Bierwagen, S. Sallis, L. F. J. Piper, M. E. Bowden, V. Shutthanandan, P. V. Sushko, and S. A. Chambers, "Perovskite Sr-doped LaCrO$_3$ as a new p-type transparent conducting oxide," Adv. Mater. **27**, 5191–5195 (2015).

[35]J. H. Jeon, T. K. Gong, Y. M. Kong, H. M. Lee, and D. Kim, "Effect of post-deposition annealing on the structural, optical and electrical properties of IGZO films," Electron. Mater. Lett. **11**, 481–484 (2015).

[36]H. Yanagi, S.-i. Inoue, K. Ueda, H. Kawazoe, H. Hosono, and N. Hamada, "Electronic structure and optoelectronic properties of transparent p-type conducting CuAlO$_2$," J. Appl. Phys. **88**, 4159 (2000).

[37]M. Dekkers, G. Rijnders, and D. H. A. Blank, "ZnIr$_2$O$_4$, a p-type transparent oxide semiconductor in the class of spinel zinc-d^6-transition metal oxide," Appl. Phys. Lett. **90**, 021903 (2007).

[38]R. Nagarajan, A. D. Draeseke, A. W. Sleight, and J. Tate, "p-type conductivity in CuCr$_{1-x}$Mg$_x$O$_2$ films and powders," J. Appl. Phys. **89**, 8022–8025 (2001).

[39]N. Ito, Y. Sato, P. K. Song, A. Kaijio, K. Inoue, and Y. Shigesato, "Electrical and optical properties of amorphous indium zinc oxide films," Thin Solid Films **496**, 99–103 (2006).

[40]E. Fortunato, D. Ginley, H. Hosono, and D. C. Paine, "Transparent conducting oxides for photovoltaics," MRS Bull. **32**, 242–247 (2007).

[41]A. V. Krukau, O. A. Vydrov, A. F. Izmaylov, and G. E. Scuseria, "Influence of the exchange screening parameter on the performance of screened hybrid functionals," J. Chem. Phys. **125**, 224106 (2006).

[42]I. Bonalde, E. Medina, M. Rodríguez, S. M. Wasim, G. Marín, C. Rincín, A. Rincín, and C. Torres, "Urbach tail, disorder, and localized modes in ternary semiconductors," Phys. Rev. B **69**, 195201 (2004).

[43]S. John, C. Soukoulis, M. H. Cohen, and E. N. Economou, "Theory of electron band tails and the urbach optical-absorption edge," Phys. Rev. Lett. **57**, 1777–1780 (1986).

[44]M. J. Wahila, K. T. Butler, Z. W. Lebens-Higgins, C. H. Hendon, A. S. Nandur, R. E. Treharne, N. F. Quackenbush, S. Sallis, K. Mason, H. Paik, D. G. Schlom, J. C. Woicik, J. Guo, D. A. Arena, B. E. White, G. W. Watson, A. Walsh, and L. F. J. Piper, "Lone-pair stabilization in transparent amorphous tin oxides: A potential route to p-type conduction pathways," Chem. Mater. **28**, 4706–4713 (2016).

[45]P. J. M. Isherwood, K. T. Butler, A. Walsh, and J. M. Walls, "A tunable amorphous p-type ternary oxide system: The highly mismatched alloy of copper tin oxide," J. Appl. Phys. **118**, 105702 (2015).

[46]G. Kresse and J. Furthmüller, "Efficient iterative schemes for *ab initio* total-energy calculations using a plane-wave basis set," Phys. Rev. B **54**, 11169–11186 (1996).

[47]P. E. Blöchl, "Projector augmented-wave method," Phys. Rev. B **50**, 17953–17979 (1994).

[48] J. P. Perdew, A. Ruzsinszky, G. I. Csonka, O. A. Vydrov, G. E. Scuseria, L. A. Constantin, X. Zhou, and K. Burke, "Restoring the density-gradient expansion for exchange in solids and surfaces," Phys. Rev. Lett. **100**, 136406 (2008).

[49] E. S. Goh, J. W. Mah, and T. L. Yoon, "Effects of Hubbard term correction on the structural parameters and electronic properties of wurtzite ZnO," Comput. Mater. Sci. **138**, 111–116 (2017); e-print arXiv:1703.02496.

[50] W. Körner, P. Gumbsch, and C. Elsässer, "Analysis of electronic subgap states in amorphous semiconductor oxides based on the example of Zn-Sn-O systems," Phys. Rev. B **86**, 165210 (2012).

[51] W. Körner and C. Elsässer, "Density-functional theory study of stability and subgap states of crystalline and amorphous Zn-Sn-O," Thin Solid Films **555**, 81–86 (2014).

[52] W. Körner, D. F. Urban, and C. Elsässer, "Generic origin of subgap states in transparent amorphous semiconductor oxides illustrated for the cases of In-Zn-O and In-Sn-O," Phys. Status Solidi A **212**, 1476–1481 (2015).

[53] E. Rucavado, Q. Jeangros, D. F. Urban, J. Holovský, Z. Remes, M. Duchamp, F. Landucci, R. E. Dunin-Borkowski, W. Körner, C. Elsässer, A. Hessler-Wyser, M. Morales-Masis, and C. Ballif, "Enhancing the optoelectronic properties of amorphous zinc tin oxide by subgap defect passivation: A theoretical and experimental demonstration," Phys. Rev. B **95**, 245204 (2017).

[54] D. Y. Cho, J. H. Kim, K. D. Na, J. Song, C. S. Hwang, B. G. Park, J. Y. Kim, C. H. Min, and S. J. Oh, "Spectroscopic evidence for limited carrier hopping interaction in amorphous ZnO thin film," Appl. Phys. Lett. **95**, 261903 (2009).

[55] D. Schmeißer, J. Haeberle, P. Barquinha, D. Gaspar, L. Pereira, R. Martins, and E. Fortunato, "Electronic structure of amorphous ZnO films," Phys. Status Solidi C **11**, 1476–1480 (2014).

[56] R. Kykyneshi, J. Zeng, and D. P. Cann, "Transparent conducting oxides based on tin oxide," in *Handbook of Transparent Conductors*, edited by D. Ginley, H. Hosono, and D. C. Paine (Springer US, 2011), Chap. 6, pp. 171–191.